11-2020

Nano-Hydroxyapatite and Nano-Hydroxyapatite/Zinc Oxide Scaffold for Bone Tissue Engineering Application

Fatemeh Heidari

Reza Bazargan-Lari

Mehdi Razavi

Farahnaz Fahimipour

Daryoosh Vashaee

See next page for additional authors

Authors

Fatemeh Heidari, Reza Bazargan-Lari, Mehdi Razavi, Farahnaz Fahimipour, Daryoosh Vashaee, and Lobat Tayebi

International Journal of Applied Ceramic Technology, Vol. 17, No. 6 (November/December 2020): 2752-2761. DOI.

Nano-Hydroxyapatite and Nano-Hydroxyapatite/Zinc Oxide Scaffold for Bone Tissue Engineering Application

Fatemeh Heidari
Department of Materials Engineering, School of Engineering, Yasouj University, Yasuj, Iran
Reza Bazargan-Lari
Department of Materials Science and Engineering, Marvdasht Branch, Islamic Azad University, Marvdasht, Iran
Mehdi Razavi
BiionixTM (Bionic Materials, Implants & Interfaces) Cluster, Department of Internal Medicine, College of Medicine, University of Central Florida, Orlando, FL
Department of Materials Science & Engineering, University of Central Florida, Orlando, FL
Farahnaz Fahimipour
Marquette University School of Dentistry, Milwaukee, WI
Dental Biomaterials Department, School of Dentistry, Tehran University of Medical Sciences, Tehran, Iran
Daryoosh Vashaee
Department of Electrical and Computer Engineering, NC State University, Raleigh, NC

Lobat Tayebi
Marquette University School of Dentistry, Milwaukee, WI

Abstract

This research aims to evaluate the mechanical properties, biocompatibility, and degradation behavior of scaffolds made of pure hydroxyapatite (HA) and HA-modified by ZnO for bone tissue engineering applications. HA and ZnO were developed using sol-gel and precipitation methods respectively. The scaffolds properties were characterized using X-ray diffraction (XRD), Fourier transform spectroscopy (FTIR), scanning electron microscopy (SEM), energy dispersive spectroscopy (EDS), transmission electron microscopy (TEM), atomic absorption (AA), and atomic force microscopy (AFM). The interaction of scaffold with cells was assessed using in vitro cell proliferation and alkaline phosphatase (ALP) assays. The obtained results indicate that the HA/ZnO scaffolds possess higher compressive strength, fracture toughness, and density—but lower hardness—when compared to the pure HA scaffolds. After immersing the scaffold in the SBF solution, more deposited apatite appeared on the HA/ZnO, which results in the rougher surface on this scaffold compared to the pure HA scaffold. Finally, the in vitro biological analysis using human osteoblast cells reveals that scaffolds are biocompatible with adequate ALP activity.

Keywords

Bioceramics, bone, nanomaterials

INTRODUCTION

Bioceramics have been widely used in medicine and dentistry. One remarkable success of bioceramics is the emergence and clinical use of bioactive ceramics.[1] Over the past 20 years, a wide range of calcium phosphates—such as hydroxyapatite (HA),[2-4] amorphous calcium phosphate,[5-8] tetra-calcium phosphate,[9] and mono-di calcium phosphate[10-12]—has been studied in both dentistry and in orthopedics fields. Micro or nanoscale HA have been investigated, and their mechanical properties have been tested.[13] Calcium phosphates are primarily used for bone replacement, since they are biocompatible, have a low density, have excellent chemical stability and are similar in chemical composition to the bone mineral phase. Among calcium phosphates, HA is stoichiometric, biocompatible, osteoconductive, nontoxic, noninflammatory, nonimmunogenic, and biologically active.[14] This means that it is capable of direct chemical bonding with living tissue.[14] Micro HA is used in the shape of thin-film coating, powder, porous scaffolds, and dense blocks.[15] Because of its bioavailability, HA can be used as the material for bone implants; over the time, it can help bone production. The bioavailability of HA can be increased by increasing its crystallinity degree and reducing its grain size.[16] The rate of calcium dissolution, however, is one of the HA's weaknesses in clinical applications that needs to be corrected.[17] Osteoconductive properties associated with HA are attributed to its dissolution behavior in the human body. Proper structural change is one of the ways to increase the dissolution rate of HA.[17]

Zinc (Zn) is one of the metal elements in the human body that is essential for bone structure and metabolism.[18] The bone mineral has the largest amount of this element (ie 160-300 ppm). Zn also plays

a role in cell differentiation, the growth and metabolism of proteins, carbohydrates, and lipids. It also plays a role in the structure of hormones and genetic transcription, while also contributing to the synthesis and degradation of nucleic acids, carbohydrates, lipids and proteins, and many vital reactions. Studies on the role of Zn on stimulating bone growth in vitro and in vivo have shown that it reduces the bone deterioration by preventing osteoclast and ALP activity.[19] Zn also stimulates collagen formation and development of bone growth proteins, such as osteocalcin, IGF-1, TGR-f, and aminoacyl-tRNA.[20] Zn ion is not only useful for bone regeneration but also is anti-inflammatory.

Zn also has antibacterial properties and is an essential metal element for cell growth and regeneration of extracellular matrix; therefore, Zn can improve the bone tissue repair process and has been used in bioactive glasses.[21] ZnO nanoparticles also exhibit antibacterial activity. The reason for the antibacterial activity of ZnO is due to its ion release or reactive oxygen species generation.[22] Recent studies have shown that the use of ZnO nanoparticles increases the proliferation of bone cells and contributes to bone growth. The above-mentioned benefits of ZnO are strongly dependent on their release behavior. Hence, the release rate of ZnO should be carefully controlled.[22]

Ching et al prepared HA nanoparticles with a wet chemical method and blended them with commercial ZnO with different weight percentages below 1% of ZnO.[23] Safari Gezaz et al prepared nano-HA particles and nano-ZnO with a sol-gel method, separately, and blended them in different weight percentages from 0% to 100% ZnO.[24] They only investigated mechanical properties, and their nanocomposite fabrication process was blending. Vijaykumar et al doped ZnO nanoparticles to HA and prepared nanofibrous particles to investigate mechanical properties and viability.[25] In this study, it is intended to modify the HA nanoparticles prepared by sol-gel method with ZnO nanoparticle precipitation. To construct the scaffolds, we used the cold isostatic pressure (CIP), and then the specimens were sintered at 1300°C. Microstructure, biodegradability, biocompatibility, and mechanical properties of scaffolds were then investigated.

MATERIALS AND METHODS

Material preparation

Hydroxyapatite (HA) synthesis

Nano-HA was prepared using the sol-gel method, as previously described.[26] Briefly, $Ca(NO_3)_2{\cdot}4H_2O$ (0.1 mol/L) and $(NH_4)_2HPO_4$ (0.06 mol/L) were dissolved in deionized water separately, and the pH of both solutions was adjusted to 11.0 by adding ammonia solution. The solution of $Ca(NO_3)_2{\cdot}4H_2O$ was dropwise added into the $(NH_4)_2HPO_4$ solution for 1 hour, and the white suspension and gelatinous precipitate were obtained. After aging for 24 hours at room temperature, the precipitates were filtered, washed several times with distilled water and absolute ethanol, dried at 80°C overnight, then calcined at 800°C for 2 hours.

Preparation of ZnO modified-HA powder

A $Zn(NO_3)_2.6H_2O$ (0.267 g, 0.897 mmol) solution was precipitated with $NaNO_3$ (1 mol/L) at room temperature and pH of 8. Nano-HA (2 g) was then added into the precipitated $Zn(OH)_2$, followed by constant stirring for 2 hours at 70°C-80°C. Finally, the white precipitates were washed with deionized water and dried at 80°C overnight. The obtained powder was calcined at 450°C for 2 hours.[27]

Preparation of ZnO modified-HA scaffolds

The prepared ZnO modified-HA powder was cold isostatic pressed (CIP) at 250 MPa. The pressed powder was then sintered at 1300°C for 2.5 hours in a box furnace at a heating rate of 5°C/min. Next, the samples in the shape of circular discs were produced for hardness or compression tests.

Material characterization

To investigate the phase composition of extracted HA powder, X-ray diffraction (XRD: Bruker-AXS-D8-Discover) analysis was carried out before and after sintering the HA. The XRD details are described in the Supplementary Material 1.

To identify the existence of organic species, along with the degree of probable dehydroxylation of HA during the heat treatment, we performed Fourier transform infrared analysis (FTIR: Shimadzu 8300). The FTIR details are described in the Supplementary Material 1.

A scanning electron microscope (SEM) equipped with energy dispersive spectroscopy (EDS) was used to examine the morphology of the powder and scaffolds. The porosity of scaffolds was also investigated by SEM.

Topography and surface roughness of the scaffolds, plus the particle size of the produced powder were measured by an atomic force microscopy (AFM; Alpha 300A WITec Germany). The non-contact mode was considered and 3D images were presented in the area measuring $1 \times 1\ \mu m^2$.

A transmission electron microscope (JEOL JEM-2100 TEM) was used to assess the nanoparticles' morphology and size in the ZnO modified HA scaffolds.

To determine ZnO within the ZnO modified HA scaffolds, an AA680 atomic absorption/flame emission spectrophotometer (Shimadzu) was used.

Mechanical properties

Mechanical properties of the samples were evaluated with compressive and hardness tests. The compressive test was performed on cylindrical samples (10 mm in diameter × 10 mm in length) using a universal testing machine (Zwick, Material Prufung, 1446e60) with a 10 kN load cell. Although the best sample for a compression test is a diameter-to-height ratio of 1/2, but in the ceramic samples, we can also test the compression with a diameter-to-height ratio of 1.[28] The crosshead speed was 0.5 mm/min. The surface area under the stress-strain curves was calculated and considered as the fracture toughness of the samples. Disc shape samples were selected for microhardness test (16 mm diameter × 4 mm height). The microhardness (Hv) of the polished sintered samples was determined via the Vickers indentation (MHV1000Z) using an applied load of 200 g with a dwell time of 10 seconds. The density of samples was measured by the Archimedes method.

In vitro biodegradability

The sintered HA samples were soaked in 20 mL of simulated body fluid (SBF) with pH 7.40 and specific ion concentrations nearly identical to those in human blood plasma (Na^+ 140.3 mm, K^+ 5.3 mm, Mg^{2+} 1.3 mm, Ca^{2+} 2.2 mm, Cl^- 148.0 mm, HCO^{3-} 4.0 mm, HPO_4^{2-} 0.8 mm, SO_4^{2-} 0.5 mm). After the samples were kept at 37°C for 28 days, they were removed from SBF, gently rinsed with distilled water and

dried at room temperature. Changes in the surface morphologies of samples before and after soaking in the SBF were characterized by SEM and EDX.

Cell culture

To sterilize the samples, they were immersed in 70% ethanol three times, followed by washing with phosphate buffer saline (PBS) for 15 min/cycle. Culture medium was prepared from Dulbecco's Modified Eagle Medium (DMEM, Sigma) supplemented with 10% fetal bovine serum (FBS, Sigma) and 1% Penicillin-Streptomycin (Invitrogen). 5×10^5 Human Osteoblast Cells (HOB, Cell Applications) were cultured on the samples immersed in growth medium. The medium was refreshed every 2 days.

The morphology of HOB cells cultured on the samples was studied by scanning electron microscopy (SEM, JEOL JSM-6510LV) after 14 days' culture. The cell culture details are described in the Supplementary Material 1.

The fluorescence intensity (Ex: 560 nm and Em: 590 nm) was measured by a spectrophotometric plate reader (Synergy HTX, BioTEK). Triplicate samples were used for this experiment.

Alkaline phosphatase activity (ALP)

ALP of HOB seeded samples was performed using an ALP assay kit (Abcam) after 14 days. The seeded cells on the samples were lysed with RIPA Lysis and Extraction Buffer (Invitrogen). 50 µL of lysate was reacted with 150 µL of p-nitrophenyl phosphate (p-NPP) for 45 minutes at 37°C. The reaction was terminated with a stop solution, and the absorbance intensity of p-nitrophenol was determined at 405 nm, using a microplate reader (Synergy HTX, BioTEK). The details of the ALP and statistical analysis are described in the Supplementary Material 1.

RESULTS AND DISCUSSION

FTIR analysis

The stretching band at 3426.89 cm^{-1} and liberation band at 632.537 cm^{-1} originate from OH^- groups. The bands located at 472.474, 568.798, 601.682, 1039.44, and 1091.51 cm^{-1} originate from $PO4^{3-}$ ions, and are weaker than the strong P-O stretching vibration due to HA stoichiometry. The bands at 1400.07 and 1614.13 cm^{-1} originate from $CO3^{2-}$ ions (Figure 1A). Carbonate ions are a common impurity in both synthetic and natural HA.[28] The FTIR spectrum of the sample that was heat-treated at 800°C is in good agreement with the spectrum reported by Heidari et al[28] for natural HA material (see Figure 1A).

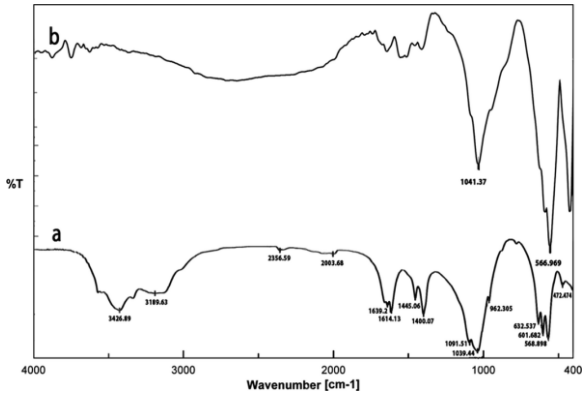

1 FTIR analysis of (A) HA, (B) HA/Zn powder

Figure 1B shows the spectra of the composite of HA/ZnO. Given that the Zn-O vibration bond occurs at a wavelength of 575 cm^{-1},[29] the sharp peak in this diagram at wavelength 566.969 cm^{-1} is related to vibration of the zinc-oxygen bond.

XRD analysis

Figure 2A,B show the XRD analysis for pure HA and HA/ZnO. The XRD pattern of these samples shows the following broad diffraction peaks at 26.172°, 28.25°, 29.1°, 31.9°, 32.35, 33°, 34.2°, 39.96°, 46.85°, 48.25°, 50.65°, 51.4°, 52.35°, 63.1°, and 53.38° (Figure 2A). All reflections are characteristics of the hexagonal phase of HA [$Ca_{10}(PO_4)_6(OH)_2$], according to the standard data (JCPDS No. 74-0566).[30] The obtained patterns are in agreement with Kim et al[31] and Heidari et al.[32,33]

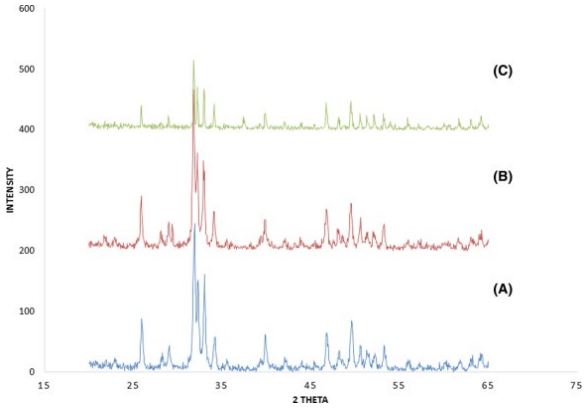

2 The XRD results for (A) HA powder synthesized by the sol-gel method; (B) HA powder synthesis by sol-gel method and modified by ZnO; (C) HA/ZnO scaffold prepared by CIP method and sintered at 1300°C

As shown in Figure 2B, the diffraction pattern does not indicate the ZnO peak, which can be due to the low percentage of ZnO in the HA/ZnO composite. Figure 2C shows the XRD pattern of HA/ZnO composite, which was prepared by a cold isostatic pressing method and followed by a sintering process at 1300°C. As shown in the XRD pattern, the main peaks of HA still exist, and no new peak related to tricalcium phosphate was detected. However, a lower peak intensity was observed from HA/ZnO composite (Figure 2C) compared to its powder (Figure 2B), which can be due to undeveloped grain growth in the samples sintered at 1300°C.[34]

Atomic absorption analysis

Atomic absorption analysis was performed on ZnO-modified HA powder. First, 0.3 g of this powder was dissolved in 25 cc solvent (chloridric acid), and the concentration of Zn^{2+} ion was estimated to be 0.191 mg/L. This estimate is for a liter of solvent equivalent to 4.77×10^{-3} mg zinc ions. As 0.02 g of powder for atomic absorption was used, the percentage of total Zn^{2+}, Ca^{2+}, and Pd^{2+} ions in the whole powder would be 0.06, 29.15, and 0.095 percent. The molecular mass of Zn is 65.4 g/mol, while the molecular mass of oxygen is 16 g/mol; therefore, the percentage of ZnO deposited on HA is equal to 81.65 × 0.016%, which is approximately 0.02%.

The molecular weight of $Zn(NO_3)_2.6H_2O$, which is equal to 297.4 g/mol, and the amount of 0.267 g of this salt was used in this study. Therefore, the Zn^{2+} contribution is 0.058%, which, in proportion to the

initial HA weight used (2 g), should be in the composite 0.028%, while according to the results of atomic absorption the Zn^{2+} concentration is equivalent to 0.016%. Thus, as much as 0.012% zinc ions are lost, which can be due to the incomplete deposition of the $Zn(OH)_2$ in the presence of HA powder after the addition of ammonia in solution.

Scanning electron microscope images

Figure 3A-C show the SEM images of HA/ZnO powder and the cross-sectional area of the pure HA and HA/ZnO composite samples sintered at a temperature of 1300°C. According to Figure 3A, the size of agglomerated powder particles is 2 ± 0.5 µm. Results show that modification of HA with ZnO reduces the porosity of HA (Figure 3B) and enhances its sinterability (Figure 3C).

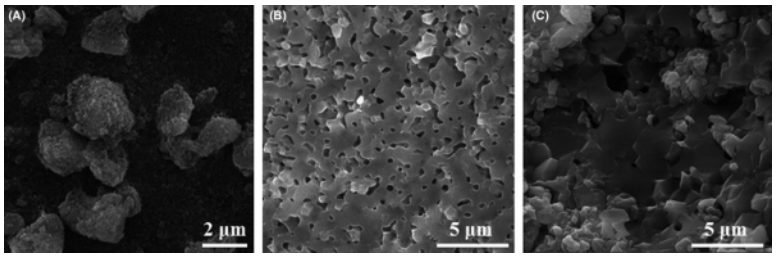

3 SEM images of (A) HA/ZnO powder (top view), (B) HA scaffold (cross-sectional view) and (C) HA/ZnO scaffold (cross-sectional view)

Transmission electron microscope images

According to TEM images, the HA/ZnO nanoparticles have a spherical shape with an average particle size of less than 80 nm (Figure 4A). In high magnification TEM images, the average size of ZnO nanoparticles on the surface of HA is 10 nm.

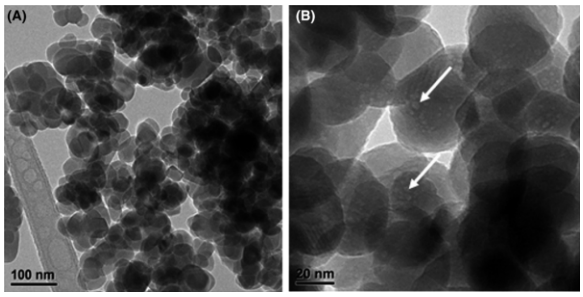

4 TEM images of HA/ZnO in (A) low and (B) high magnification, showing the morphology and size of nanoparticles

Mechanical testing

Heidari *et al* reported that HA samples extracted from the cattle bone—pressed with a CIP method and sintered at 1300°C—have a compressive strength of 3.25 aPM and a fracture toughness of 0.3 aPM.[28] However, in this study, with the same manufacturing conditions, the compressive strength of the pure HA sample obtained is 22.4 MPa, while the fracture toughness is reduced to 0.168 MPa (Table 1). Furthermore, hardness in these specimens has been shown to increase by 1 GPa than those made from natural HA. These changes are likely due to the HA powder, which had been synthesized by the sol-gel method, and the size of the powder was smaller compared to HA used in our previous study.[28] Teh et al reported that ZnO increases the density of HA. Increasing the temperature of the sintering also

increases the density. Up to 1250°C, the addition of 0.1% ZnO to HA increases the density to 99.1%. This causes an increase in fracture toughness by 0.2 $MPam^{1/2}$, while the hardness remains constant.[35] Addition of 0.02% ZnO to HA results in a reduction in hardness (from 4.26 to 3.14 GPa), an increase in density (from 2.83 to 2.86 g/cm^3), an increase in compressive strength (from 22.4 to 23.2 MPa), and an increase the fracture toughness (from 0.168 to 0.232 MPa) of the samples (Table 1). Hence, our results show that ZnO increases the fracture energy of the samples due to the condensation of the samples under the same conditions of production.

1 TABLE Mechanical properties of HA and ZnO modified HA scaffolds

Density (g/cm^3)	**Hardness (GPa)**	**Fracture TOUGHNESS (MPa)**	**Fracture strength (MPa)**	
2.83	4.26	0.168	22.4	HA
2.86	3.14	0.232	23.2	HA/ZnO

Immersion in SBF solution

Figure 5A shows the surface topography of the HA powder prepared by the sol-gel method. The results of the AFM analysis indicates that the HA particle size is in the range of 90 to 110 nm. This range of particle size is much smaller than the particle size range of HA powder extracted from the cattle bone reported by Heidari et al, which was about 5 µm.[32]

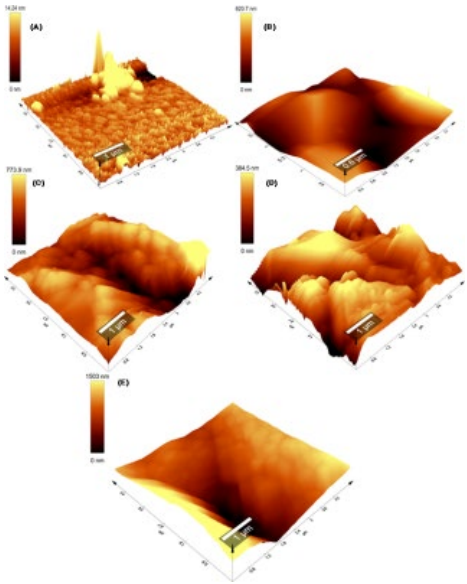

5 Analysis of surface topography using AFM from (A) sol-gel synthesized HA powder, (B) surface of pure HA scaffold before immersion, (C) surface of HA/ZnO scaffold before immersion, (D) surface of pure HA scaffold after immersion, and (E) surface of HA/ZnO scaffold after immersion in the SBF solution

The surface roughness of the HA scaffolds is shown in Figure 5B. The mean roughness of the samples before and after immersion in SBF indicated in Table 2. Figure 5C shows the AFM graph of HA/ZnO, when the roughness of ZnO deposited on HA has increased from 620.7 to 773.9 nm (Table 2). Figure 5D shows the AFM graph of the surface of the pure HA sample after immersion. Surface roughness decreases by 236.2 nm, compared to before immersion. Figure 5E shows the surface of the HA/ZnO sample. The surface roughness in this sample has increased from 773.9 to 1503 nm (Table 2). Our

results show that ZnO can increase apatite deposition on the surface of HA scaffolds. Usually at roughness more than 50 nm, van der Waals forces are the main factor; while at closer distances (10-20 nm), a combination of both van der Waals forces and electrostatic interactions controls cell adhesion.[36] For metals used in medical implants, the desired surface roughness is usually below 10 nm.[37] Rough surface promotes friction, thus reduces the mobility of the bacteria; this sessile environment facilitates the biofilm growth.[38] Hence, HA and HA/ZnO have a significant surface roughness and can be a good place for cell proliferation.

2 TABLE The amount of roughness of surface samples

Samples	**Surface Roughness Before Immersion (nm)**	**Surface Roughness After Immersion (nm)**	**Change in Roughness (nm)**
HA	620.7	384.5	−236.2
HA/ZnO	773.9	1503	+729.1

Figure 6A,B indicate the SEM images of HA and HA/ZnO after 28 days immersion in SBF. This image shows that apatite deposition on pure HA is completely uniform, but Figure 6B indicates the increase in the surface roughness of HA/ZnO.

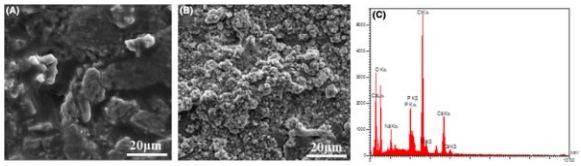

6 SEM images from the surface of the scaffold after 28 d of immersion in SBF solution, (A) pure HA, (B) HA/ZnO, (C) EDS analysis of the deposited layer on the surface of HA/ZnO scaffold

The formed apatite has been further analyzed and confirmed by EDS, showing the main elements are calcium and phosphorus (Figure 6C). Also, other elements (chlorine and sodium) are detected in our EDS analysis, which can be due to the NaCl in the SBF solution.

Cell culture

ALP is believed to be upregulated in the early stages of biomineralization in order to form a large pool of inorganic phosphate from which HA can be mineralized.[39] After the onset of mineralization, ALP is no longer needed, and therefore, cellular levels of the enzyme drop before a mature mineralized matrix are formed.[40] Figure 7 shows the results of ALP after 14 days. The statistical analysis showed that the ALP activity for pure HA sample was higher than the HA/ZnO ones.

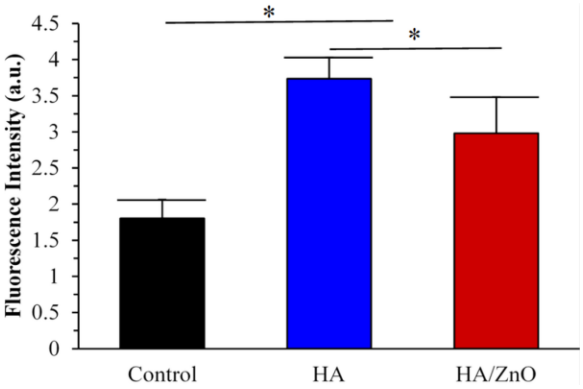

7 ALP assessment on HA and HA/ZnO scaffolds (14 d)

Figure 8 shows the proliferation of human osteoblast cells on the surface of the scaffold. Darker graphs appear after 7 days, and more explicit graphs after 14 days in the culture medium. The density of the cells cultured on both samples significantly increased after 14 days than 7 days. Generally, the proliferation of cells on pure HA was higher than that of HA/ZnO, however, both samples show significantly higher cellular viability after 14 days compared to the control sample ($P < .05$).

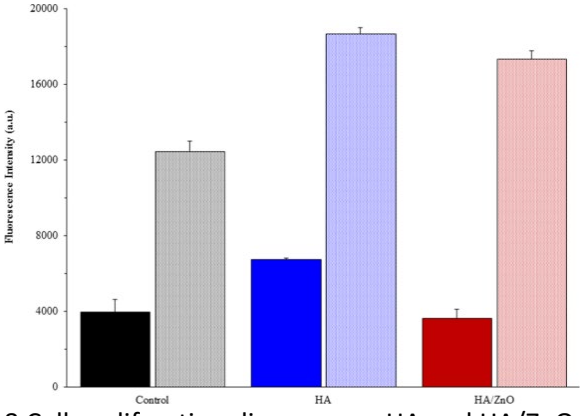

8 Cell proliferation diagrams on HA and HA/ZnO scaffolds after 7 (darker) and 14 d (clearer graphs)

In such conditions, we should know that at some concentrations, Zn ions could also have adverse effects on the cells. Although Jafarirad et al showed that the negative charge of ZnO nanoparticles at concentrations of 0.05 and 0.1 mg/mL induced very low toxicity on cancer cell lines, another study reported toxicity of ZnO particles towards epithelial cells.[41,42]

One limitation of our study is not considering the amount of deposited and released Zn ion from our samples. Grenho et al measured the Zn ion release and showed a slight increase of the release of Zn ions in nano-HA granules with 2% ZnO from 0.30 to 0.38 ppm, from day 1 to day 3 respectively. This amount in day 3 caused an inhibitory effect on MG63 cells and caused lower cell proliferation [43]. Also, Li *et al* reported good reproduction behavior of L929 cell line at lower ZnO nanowires concentration and considerable viability drop (~50%) at concentrations close to 100 µg/mL.[44] One study showed that structural modifications in lattices of ZnO could decrease its solubility and, therefore, reduce its cytotoxicity.[45] Future studies are recommended for measurement of the released Zn ion from HA/ZnO constructs and screening the best concentration. Furthermore, the efficacy of these samples against different bacteria might be assessed.

Figure 9 shows SEM images of human osteoblast cells attached to the surface of the specimens after 14 syad, confirming the biocompatibility of our HA and HA/ZnO scaffolds.

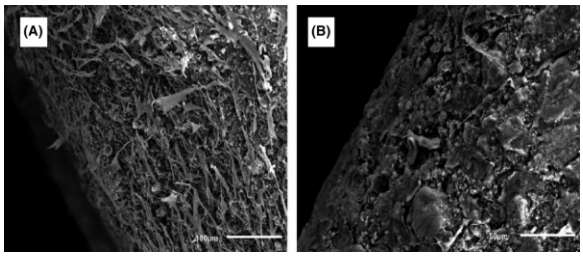

9 SEM images from the cells attached surface of the specimens after 14 d of culture: (A) pure HA scaffold, (B) HA/ZnO scaffold

CONCLUSION

HA powder was synthesized by sol-gel method and modified with ZnO deposition. Scaffolds were then made using the CIP method, followed by sintering at 1300°C. Modification of HA with ZnO increases the compressive strength, fracture toughness and density. Results of surface topography show that the HA/ZnO scaffold is rougher than the pure HA one. After immersion in the SBF solution, more apatite is deposited on the surface of the HA/ZnO compared to HA bioscaffold. The results of cell attachment and proliferation prove the biocompatibility of our HA/ZnO bioscaffolds.

ACKNOWLEDGMENT

The authors thank the financial support from Iran National Science Foundation, INSF (Grant No. 95838463).

GRAPH: Supplementary Material

REFERENCES

1. *Sebdani MM, Fathi MH. Preparation and characterization of hydroxyapatite–forsterite–bioactive glass nanocomposite coatings for biomedical applications. Ceram Int. 2012 ; 38 (2): 1325 – 30.*
2. *Vu AA, Robertson SF. Mechanical and biological properties of ZnO, SiO 2, and Ag 2 O doped plasma sprayed hydroxyapatite coating for orthopaedic and dental applications. Acta Biomater. 2019 ; 92 : 325 – 35.*
3. *Henry MG, Cai L, Liu X, Zhang L, Dong J, Chen L, et al. Roles of hydroxyapatite allocation and microgroove dimension in promoting preosteoblastic cell functions on photocured polymer nanocomposites through nuclear distribution and alignment. Langmuir. 2015 ; 31 (9): 2851 – 60.*
4. *Li J, Liu X. Strontium-substituted hydroxyapatite stimulates osteogenesis on poly(propylene fumarate) nanocomposite scaffolds. J Biomed Materer Res A. 2019 ; 107 (3): 631 – 42.*
5. *Safronova TV, Mukhin EA, Putlyaev VI, Knotko AV, Evdokimov PV, Shatalova TB, et al. Amorphous calcium phosphate powder synthesized from calcium acetate and polyphosphoric acid for bioceramics application. Ceram Int. 2017 ; 43 (1, Part B): 1310 – 7.*

6. *Shafiei S, Omidi M, Nasehi F, Golzar H, Mohammadrezaei D, Rezai M, et al. Egg shell-derived calcium phosphate/carbon dot nanofibrous scaffolds for bone tissue engineering: Fabrication and characterization. Mater Sci Eng, C. 2019 ; 100 : 564 – 75.*
7. *Bussola Tovani C, Gloter A. Formation of stable strontium-rich amorphous calcium phosphate: Possible effects on bone mineral. Acta Biomater. 2019 ; 92 : 315 – 24.*
8. *Gelli R, Ridi F. The importance of being amorphous: calcium and magnesium phosphates in the human body. Adv Coll Interface Sci. 2019 ; 269 : 219 – 35.*
9. *Xu HHK, Weir MD. Calcium and phosphate ion releasing composite: Effect of pH on release and mechanical properties. Dental Mater. 2009 ; 25 (4): 535 – 42.*
10. *Xu HHK, Sun L. Effects of incorporating nanosized calcium phosphate particles on properties of whisker-reinforced dental composites. J Biomed Mater Res B Appl Biomater. 2007 ; 81 (1): 116 – 25.*
11. *Xu HHK, Sun L, Weir MD, Antonucci JM, Takagi S, Chow LC, et al. Nano DCPA-whisker composites with high strength and Ca and PO(4) release. J Dent Res. 2006 ; 85 (8): 722 – 7.*
12. *Xu HHK, Moreau J. Strength and fluoride release characteristics of a calcium fluoride based dental nanocomposite. Biomaterials. 2008 ; 29 (32): 4261 – 7.*
13. *Aljabo A, Abou Neel EA. Development of dental composites with reactive fillers that promote precipitation of antibacterial-hydroxyapatite layers. Mater Sci Eng, C. 2016 ; 60 : 285 – 92.*
14. *Currey J. Sacrificial bonds heal bone. Nature. 2001 ; 414 : 699.*
15. *Murugan R, Ramakrishna S. Coupling of therapeutic molecules onto surface modified coralline hydroxyapatite. Biomaterials. 2004 ; 25 (15): 3073 – 80.*
16. *Fathi MH, Hanifi A. Preparation and bioactivity evaluation of bone-like hydroxyapatite nanopowder. J Mater Process Technol. 2008 ; 202 (1): 536 – 42.*
17. *Latifi SM, Fathi MH. Simultaneous structural and surface modifications of nanophase hydroxyapatite for improving its dissolution and bioactivity. Ceram Int. 2016 ; 42 (5): 6355 – 9.*
18. *Tapiero H, Tew KD. Trace elements in human physiology and pathology: zinc and metallothioneins. Biomed Pharmacother. 2003 ; 57 (9): 399 – 411.*
19. *Yamaguchi M, Yamaguchi R. Action of zinc on bone metabolism in rats: Increases in alkaline phosphatase activity and DNA content. Biochem Pharmacol. 1986 ; 35 (5): 773 – 7.*
20. *Franceschi RT, Iyer BS. Relationship between collagen synthesis and expression of the osteoblast phenotype in MC3T3-E1 cells. J Bone Mineral Res. 1992 ; 7 (2): 235 – 46.*
21. *Chen L, Dai Y. Structure, physical properties, crystallization and sintering of iron-calcium-aluminosilicate glasses with different amounts of ZnO. J Non-Cryst Solids. 2016 ; 452 : 45 – 9.*
22. *Cheng K, Guan ZH, Weng W, Wang H, Lin J, Du P, et al. Hydroxyapatite/ZnO-nanorod composite coatings with adjustable hydrophilicity and Zn release ability. Thin Solid Films. 2013 ; 544 : 260 – 4.*
23. *Ching TY, Singh R. The effects of zinc oxide on the sinterability of hydroxyapatite. in 2016 International Conference on Applied System Innovation (ICASI); 2016.*
24. *Safari Gezaz M, Mohammadi AS. Investigation of structural properties of hydroxyapatite/ zinc oxide nanocomposites; an alternative candidate for replacement in recovery of bones in load-tolerating areas. Mater Chem Phys. 2019 ; 226 : 169 – 76.*

25. *Gnaneshwar PV, Sudakaran SHV, Abisegapriyan S, Sherine J, Ramakrishna S, Rahim MH, et al. Ramification of zinc oxide doped hydroxyapatite biocomposites for the mineralization of osteoblasts. Mater Sci Eng, C. 2019 ; 96 : 337 – 46.*
26. *Monmaturapoj N. Nano-size hydroxyapatite powders preparation by wet-chemical precipitation route. Metals, Mater Miner. 2008 ; 18 (1): 15 – 20.*
27. *Tavakolian E, Tashkhourian J. Ethanol electrooxidation at carbon paste electrode modified with Pd–ZnO nanoparticles. Sensors Actuators B: Chem. 2016 ; 230 : 87 – 93.*
28. *Heidari F, Razavi M. Investigation of mechanical properties of natural hydroxyapatite samples prepared by cold isostatic pressing method. J Alloy Compd. 2017 ; 693 : 1150 – 6.*
29. *Buazar F, Alipourian S. Photodegradation of odorous 2-mercaptobenzoxazole through zinc oxide/hydroxyapatite nanocomposite. Applied Nanosci. 2015 ; 5 (6): 719 – 29.*
30. *Kumar A, Biswas K, Basu B. On the toughness enhancement in hydroxyapatite-based composites. Acta Mater. 2013 ; 61 (14): 5198 – 215.*
31. *Kim YG, Seo DS. Dissolution of synthetic and bovine bone-derived hydroxyapatites fabricated by hot-pressing. Appl Surf Sci. 2008 ; 255 (2): 589 – 92.*
32. *Heidari F, Bahrololoom ME. In situ preparation of iron oxide nanoparticles in natural hydroxyapatite/chitosan matrix for bone tissue engineering application. Ceram Int. 2015 ; 41 (2, Part B): 3094 – 100.*
33. *Heidari F, Razavi M, Bahrololoom ME, Bazarganlari R, Vashaee D, Kotturi H, et al. Mechanical properties of natural chitosan/hydroxyapatite/magnetite nanocomposites for tissue engineering applications. Mater Sci Eng, C. 2016 ; 65 : 338 – 44.*
34. *Fu Y, Tao Z. Weibull distribution of the fracture strength of 99% alumina ceramic reshaped by cold isostatic pressing. Ceram Int. 2014 ; 40 (6): 7661 – 7.*
35. *Teh YC, Singh R. The effects of zinc oxide on the sinterability of hydroxyapatite. International Conference on Applied System Innovation (ICASI); 2016. p. 1 – 4.*
36. *Percival SL, Knottenbelt L. Introduction to biofilms, in biofilms and veterinary medicine. Berlin Heidelberg : Springer Berlin, Heidelberg ; 2011. p. 41 – 68.*
37. *Mendonca G, Mendonca DBS. Advancing dental implant surface technology–from micron- to nanotopography. Biomaterials. 2008 ; 29 (28): 3822 – 35.*
38. *Golabi M, Turner APF. Tunable conjugated polymers for bacterial differentiation. Sensors Actuators B: Chem. 2016 ; 222 : 839 – 48.*
39. *Anderson HC. Molecular biology of matrix vesicles. Clin Orthop Relat Res. 1995 ; 314 : 266 – 80.*
40. *Boyan BD, Schwartz Z. Cell maturation-specific autocrine/paracrine regulation of matrix vesicles. Bone Miner. 1992 ; 17 (2): 263 – 8.*
41. *Cepin M, Hribar G. Morphological impact of zinc oxide particles on the antibacterial activity and human epithelia toxicity. Mater Sci Eng C: Mater Biol Appl. 2015 ; 52 : 204 – 11.*
42. *Jafarirad S, Mehrabi M. Biofabrication of zinc oxide nanoparticles using fruit extract of Rosa canina and their toxic potential against bacteria: a mechanistic approach. Mater Sci Eng C: Mater Biol Applications. 2016 ; 59 : 296 – 302.*
43. *Grenho L, Salgado CL. Antibacterial activity and biocompatibility of three-dimensional nanostructured porous granules of hydroxyapatite and zinc oxide nanoparticles—anin vitroandin vivostudy. Nanotechnology. 2015 ; 26 (31): 315101.*

44. *Li Z, Yang R. Cellular level biocompatibility and biosafety of ZnO nanowires. J Phys Chem C. 2008 ; 112 (51): 20114 – 7.*
45. *Ghaderi-Shekhi Abadi P, Shirazi FH. Influence of formulation of ZnO nanoblokes containing metallic ions dopants on their cytotoxicity and protective factors: An in vitro study on human skin cells exposed to UVA radiation. Toxicology Rep. 2018 ; 5 : 468 – 79.*